PCCP

PAPER

Cite this: *Phys. Chem. Chem. Phys.*, 2017, **19**, 21507

Hydrogenated carbon nanotube-based spin caloritronics†

Hong-Li Zeng,[ab] Yan-Dong Guo,[bc]* Xiao-Hong Yan*[abcd] and Jie Zhou[bc]

Received 2nd May 2017,
Accepted 18th July 2017

DOI: 10.1039/c7cp02862h

rsc.li/pccp

Spin caloritronics has drawn much attention as it combines thermoelectrics and spintronics together. Carbon-based structures, such as graphene, have been found to exhibit different kinds of spin caloritronic features. However, a study of spin caloritronics in carbon nanotubes (CNTs) is still lacking. Using first-principles calculations, we investigate the spin-Seebeck effect (SSE) in partially hydrogenated CNTs. It is found that linear hydrogenation could make CNTs acquire magnetism and exhibit the spin-Seebeck effect. Moreover, an odd–even effect of the SSE is observed, where the even cases could be used as spin-Seebeck diodes. Further analysis shows that, it is induced by the difference of band structures, where the band structure of a tube is a combination of that of graphene-nanoribbon parts "divided" by hydrogenation. This mechanism could be extended to nanotubes with different diameters, showing great application potential. We believe that our results are very useful for the development of nanotube-based spin caloritronic devices.

Introduction

To reduce the dimensions and energy consumption, as well as to increase the operating speed, there is considerable interest in utilizing the waste energy, *e.g.*, dissipating heat, in electronic devices.[1–3] On the other hand, spintronics shows great application potential in nanoelectronic devices due to the low energy consumption and high speed.[4–6] Recently, an emerging field called spin caloritronics has drawn much attention, as it combines thermoelectrics and spintronics together.[7] A big breakthrough in spin caloritronics is the discovery of the spin-Seebeck effect (SSE) in experiments,[8] where a temperature gradient could be used to generate spin currents without applying an electrical bias. The currents with opposite spins (up and down) would flow in opposite directions.[9–11] Related devices for practical application have also been proposed, such as spin-Seebeck diodes.[12–14] These developments pave the way for applying thermal-induced spin current in transferring and processing information.

Carbon-based materials, such as magnetic fullerene derivatives, are considered to be one of the most promising candidates for future spin-related devices.[15,16] Among them, graphene has been found to exhibit different kinds of spin caloritronics-related phenomena.[11,17–22] Carbon nanotubes (CNTs), formed by rolling graphene sheets, have also been extensively investigated in thermoelectrics and show various features.[3] However, as far as we know, they are all spin independent, not taking advantage of spintronics.[3,23–25] The study of spin dependent-thermoelectrics, *i.e.*, spin caloritronics, in CNTs is still lacking. Actually, the key problem lies in the absence of a magnetic moment in CNTs, whereas the edges in graphene nanoribbons (GNRs) could induce magnetism. Recently, it was reported that partial hydrogenation could create magnetism in carbon-based structures.[26,27] Inspired by that, we constructed partially hydrogenated carbon nanotubes (PHCNTs) and found that they exhibit interesting electronic and SSE properties.

In this work, we focus on the ferromagnetic (FM) state of PHCNTs (as the FM state can be stabilized by a magnetic field[28,29]) and study their magnetism, as well as the SSE. Besides the normal SSE behavior, an odd–even effect of the SSE is discovered, where the even cases could be used as spin-Seebeck diodes. Further analysis shows that, it is the difference in band structures due to the edge of the GNR parts that results in the odd–even effect. It should be noted that our PHCNT structure involves carbon and hydrogen atoms only. This will be quite conducive to the device application, as the structures are chemically inert, compatible with carbon components, and easy to fabricate. In addition, the SSE and spin-Seebeck diodes are realized and manipulated without the need for an electric field or gate voltage, and could be extended to nanotubes with different diameters, showing great application potential.

[a] *College of Natural Science, Nanjing University of Posts and Telecommunications, Nanjing 210046, China*
[b] *Key Laboratory of Radio Frequency and Micro–Nano Electronics of Jiangsu Province, Nanjing 210023, China*
[c] *College of Electronic Science and Engineering, Nanjing University of Posts and Telecommunications, Nanjing 210046, China. E-mail: yandongguo@njupt.edu.cn*
[d] *College of Science, Nanjing University of Aeronautics and Astronautics, Nanjing 210016, China*

† Electronic supplementary information (ESI) available. See DOI: 10.1039/c7cp02862h

Methodology

To investigate the transport properties, density functional theory (DFT) calculations combined with the nonequilibrium Green's function (NEGF) are performed using the Atomistix Toolkit package.[30,31] To simulate the electronic properties of different spin channels, spin-polarized calculations are performed. The mesh cutoff energy is set to be 150 Ry, with a $1 \times 1 \times 100$ k-point mesh in the Monkhorst–Park scheme for two-probe systems.[32] For bulk systems (not two-probe ones), the k-point mesh is $1 \times 1 \times 13$. The convergence tolerance for energy in self-consistent field calculations is 4×10^{-5} Hartree. We use Perdew–Burke–Ernzerhof (PBE) formulation of the generalized gradient approximation (GGA) as the exchange–correlation functional.[33] The double-zeta polarized basis set (DZP) is chosen to be the local numerical orbitals. In the calculations, the core electrons (like $1s^2$ in carbon), as well as their interactions with valence electrons, are described by the Fritz-Haber-Institute norm-conserving pseudopotentials. The eigenfunctions of the Kohn–Sham Hamiltonian are expanded in a linear combination of atomic orbitals (LCAO). In a two-probe system, the whole device can be divided into three parts, *i.e.*, the left and right leads, and the scattering region. The left/right lead is semi-infinite. To prevent the interaction with adjacent images, a supercell with sufficient vacuum space (more than 10 Å) is employed. Before transport calculations, hydrogenated nanotubes are fully optimized until all the forces are less than 0.02 eV Å^{-1}. In the NEGF scheme, the spin-dependent transmission probability through the two-probe system is calculated by

$$T_{\uparrow/\downarrow}(E) = \mathrm{Tr}[\Gamma_{\mathrm{L}}(E)G^{\mathrm{R}}_{\uparrow/\downarrow}(E)\Gamma_{\mathrm{R}}(E)G^{\mathrm{A}}_{\uparrow/\downarrow}(E)], \quad (1)$$

where $G^{\mathrm{A/R}}_{\uparrow/\downarrow}(E)$ is the spin-dependent advanced or retarded Green's function for the scattering region (E represents energy) and $\Gamma_{\mathrm{L/R}}$ is the coupling matrix between this region and the left/right electrode. For instance, $T_{\uparrow}(E)$ stands for the probability that an up-spin electron with energy E is transmitted from one electrode to another (it will become a ratio for many electrons). The spin-dependent current is obtained through the Landauer–Büttiker formula

$$I_{\uparrow/\downarrow} = \frac{e}{h}\int_{-\infty}^{\infty}[f_{\mathrm{L}}(E,T_{\mathrm{L}}) - f_{\mathrm{R}}(E,T_{\mathrm{R}})]T_{\uparrow/\downarrow}(E)\mathrm{d}E, \quad (2)$$

where $f_{\mathrm{L/R}}(E,T_{\mathrm{L/R}})$ is the Fermi function in the left/right electrode and $T_{\mathrm{L/R}}$ represents the temperature of the left/right electrode. Moreover, e is the elementary charge and h is the Planck constant. As an example, $I_{\uparrow}$ stands for the current contributed solely by the flow of up-spin electrons.

Results and discussion

Since the discovery of the SSE, numerous studies have been conducted on it. Besides graphene, the SSE has been found and studied in a wide range of materials and structures, *e.g.*, silicene, monolayer MoS_2 and blue phosphorene.[34–36] However, as far as we know, there is no report on the SSE in carbon nanotubes. The key reason is that there is no magnetism in CNTs. As is well known, there is also no magnetic moment in the pristine graphene.

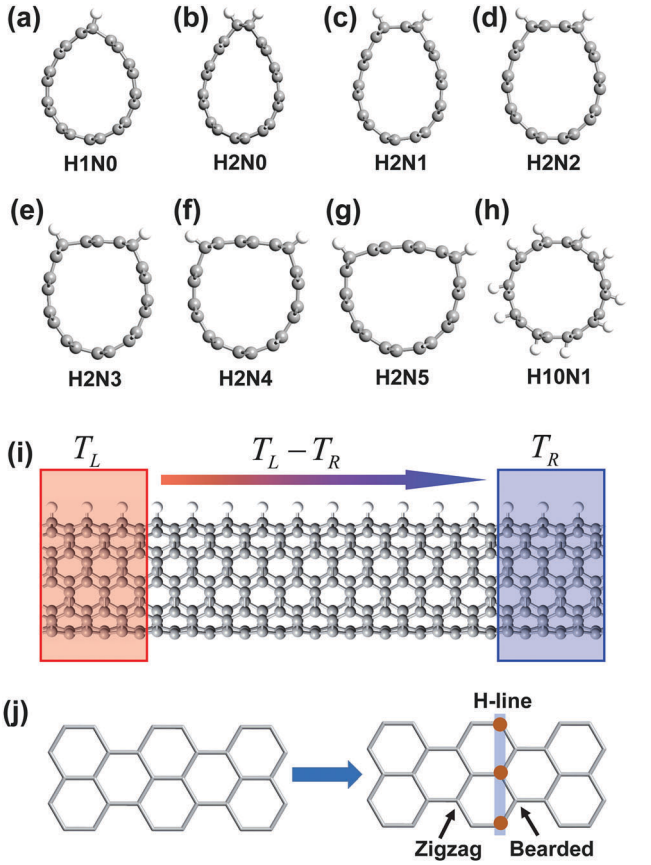

Fig. 1 (a–h) The cross-sectional views of two-probe systems of H1N0, H2N0, H2N1, H2N2, H3N3, H2N4, H2N5 and H10N1, respectively. As an example, H2N3 in (e) stands for the case that two hydrogen atoms per unit cell absorb on the (5,5) nanotube with a three-carbon-atom spacing, forming two infinite straight lines of H atoms along the axis of the tube. (i) The setup of the partially hydrogenated carbon nanotube-based thermal spin device. T_{L} and T_{R} represent the temperatures of the left and right leads respectively. And T_{LR} represents the difference between them, *i.e.*, $T_{\mathrm{L}} - T_{\mathrm{R}}$. (j) The illustration of the linear hydrogenation of a single H-line. A zigzag and a bearded edge are created on each side of the H-line.

After cutting, GNRs acquire magnetism due to the edge states, and it makes GNRs exhibit various spin caloritronics features.[11,18–22] A carbon nanotube is constructed by rolling up graphene, but it has no edge (and no corresponding magnetism). Creating magnetism is the first step to study the SSE in CNTs. Recently, it was reported that, hydrogenation in CNTs could create edge-states like that in graphene, without the need for unzipping of the CNT.[27] Moreover, linear hydrogenation in CNTs is proved to be realizable experimentally.[27,37] Based on this, we constructed eight kinds of PHCNT devices based on (5,5) nanotubes, and the cross sections of them are shown in Fig. 1(a)–(h) respectively. For simplicity sake, we use HxNy to denote a PHCNT which has x lines of adsorbed H atoms with y lines of C atoms in the interval of H-lines. For example, H2N3 represents the PHCNT structure shown in Fig. 1(e), which has two H-lines with three C-lines in the interval. The whole setup of the two-probe device is shown in Fig. 1(i). It can be divided into three parts, *i.e.*, the left and right leads and the central region.

The temperatures of the left and right leads are T_L/T_R respectively, and their difference is $T_{LR} = T_L - T_R$.

After hydrogen adsorption, the nanotube would no longer be round as the axisymmetry is broken. For instance, by single H-line hydrogenation, the H1N0 configuration in Fig. 1(a) exhibits a pear-like shape. This single H-line divides the π-bond lattices into "two parts", creating a zigzag and a bearded (Klein) π-edge on each side of the H-line,[37] as shown in Fig. 1(j). Like graphene, nanotubes are constructed by benzenoid aromatic rings. We find that linear hydrogenation successfully makes our CNTs acquire magnetism on the H-dividing edges. Calculations show that the ground state of each PHCNT is either FM or antiferromagnetic (AFM), but not nonmagnetic. Although FM is not the ground state for every configuration, it can be stabilized by an external magnetic field.[28,29,38] Thus, the FM state is realizable in practice. Besides, the anisotropy effect could assist in preserving the spin ordering state at finite temperature.[38–41] So, in a realistic situation, good viability of ferromagnetic state can be expected. In the present work, we focus on the FM state (the energetically favorable state) of the PHCNT (the discussion on the viability of FM in detail can be found in the ESI†). To observe the magnetism more clearly, we calculate the spin charge density magnetization (SCDM, *i.e.*, spin-up charge density minus spin-down charge density). The inset in Fig. 2(a) shows the isovalue surfaces of SCDM for H1N0. The isovalue surface exhibits spherical geometries around atoms. A large size of it suggests large magnetization and a small size indicates small magnetization.

According to eqn (2), we calculate the spin-dependent currents *versus* T_L with various T_{LR} for H1N0, as shown in Fig. 2(a). For all the values of T_{LR}, there is no spin-up or spin-down current when T_L is smaller than 200 K. That means in this range of T_L, there is no thermal-induced spin current, no matter how much the temperature difference (T_{LR}) is. Apparently, there is a threshold temperature T_{th} at about 200 K for both spin-up and spin-down currents. When T_L is larger than 200 K, both spin-up and spin-down currents grow larger with increasing T_L. But they split with opposite signs, *i.e.*, the spin-up currents are positive and the spin-down currents are negative. This means they flow in opposite directions in the nanotube. That is actually the SSE.[8] Moreover, the spin-up or spin-down current grows larger with the increase of T_{LR} (see Fig. 2(a)). For instance, the currents of T_{LR} = 20, 40 and 60 K for T_L = 400 K are 11.8, 21.8 and 30.0 nA, respectively. Compared with that in GNRs,[19] the spin-Seebeck currents in our nanotube system are much larger, implicating better application potential. Note that, in practical application, temperature is quite important. Here, in our calculations, the T_L increases to 600 K. It has been reported that spin injection, accumulation and precession in Si-based structures are realized at temperatures up to 500 K. In addition, for carbon systems, both theoretical and experimental studies show that magnetism with high Curie temperature, above room temperature (even larger than 500 K), is possible.[42–46]

To illustrate the underlying mechanism of the phenomenon, we plot the Fermi distributions of the left and right leads in Fig. 3(a) and (b) respectively, which are determined by the temperatures of the leads. In the SSE, the spin-current is closely

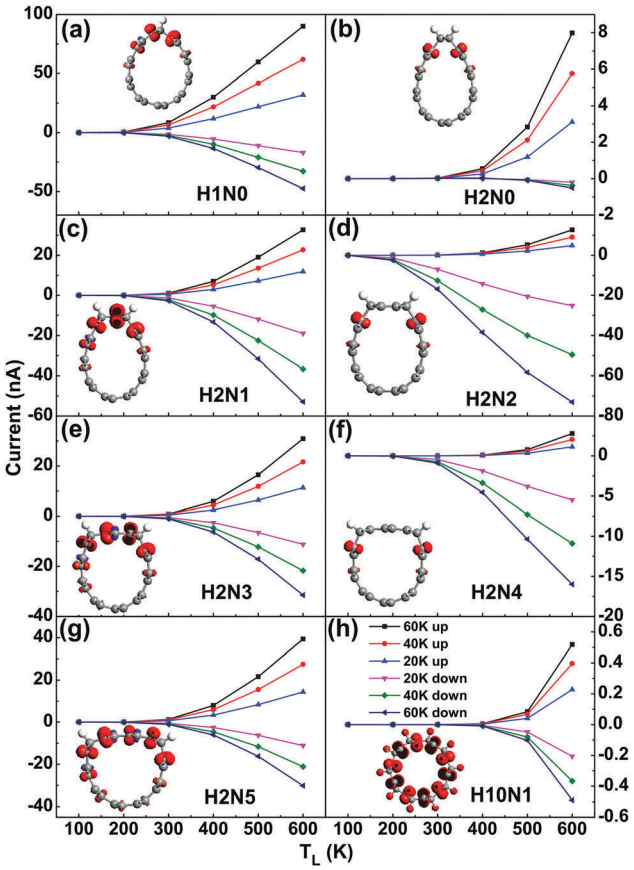

Fig. 2 The spin dependent currents *versus* T_L for different T_{LR} ($T_{LR} = T_L - T_R$ = 20, 40 and 60 K). The directions of the spin-up and spin-down currents are opposite, which is actually the SSE. Panels (a–h) correspond to the systems of H1N0, H2N0, H2N1, H2N2, H2N3, H2N4, H2N5 and H10N1, respectively. The inset in each figure shows the corresponding configurations and their isovalue surfaces of the spin charge density magnetization (*i.e.*, spin-up charge density minus spin-down charge density) under ferromagnetic state. Red (dark) and blue (light) represent spin-up polarized (positive value) and spin-down polarized (negative value), respectively, with the isovalue of 0.01 e Å^{-3}. The isovalue surface exhibits spherical geometries around atoms. A large size of it suggests large magnetization and a small size indicates small magnetization.

related to the difference of Fermi distributions between the two leads, *i.e.*, $f_L(E,T_L) - f_R(E,T_R)$. To see it more clearly, we plot this difference for the case of T_L = 400 K and T_{LR} = 60 K (as an example), as shown in Fig. 3(c). Due to such a difference, the higher-energy carriers (blue ones above E_F) would flow from the left lead to the right lead, contributing to an electron current I_e.[19] On the other hand, the lower-energy carriers (orange ones below E_F) would flow in the opposite direction, contributing to a hole current I_h. According to eqn (2), if the transmission is energy independent for each spin, the I_e and I_h currents will be equal (resulting in a zero net current) and no SSE will appear. However, for H1N0, the spin-dependent transmission is energy dependent, as shown in Fig. 3(d). For spin-down, the transmission is zero when $E < 0.15$ eV, and non-zero for $E > 0.15$ eV. In contrast, for spin-up, the transmission is zero when $E > -0.13$ eV, and non-zero for $E < -0.13$ eV. Around the Fermi level, there is a transmission gap. Actually, these

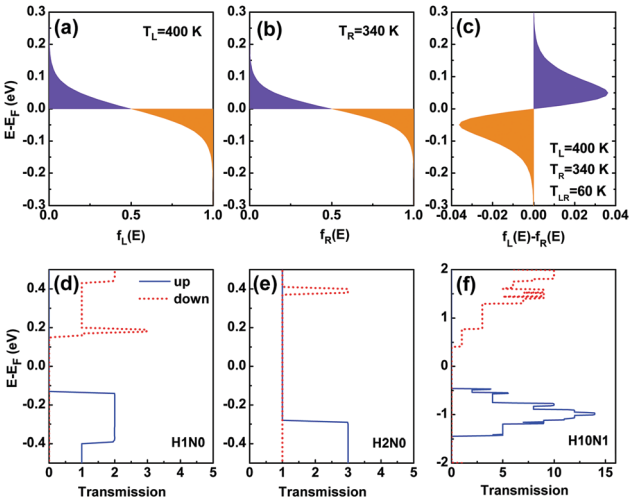

Fig. 3 The Fermi distributions of the left (a) and right (b) leads, where T_L = 400 K and T_R = 340 K. (c) The difference of the Fermi distributions between the left and right leads, *i.e.*, f_L (T = 400 K) − f_R (T = 340 K). (d–f) The spin dependent transmission spectra for H1N0, H2N0 and H10N1 systems respectively, where T_L = 400 K and T_R = 340 K (T_{LR} = 60 K). Solid blue line: spin-up; dashed red line: spin-down.

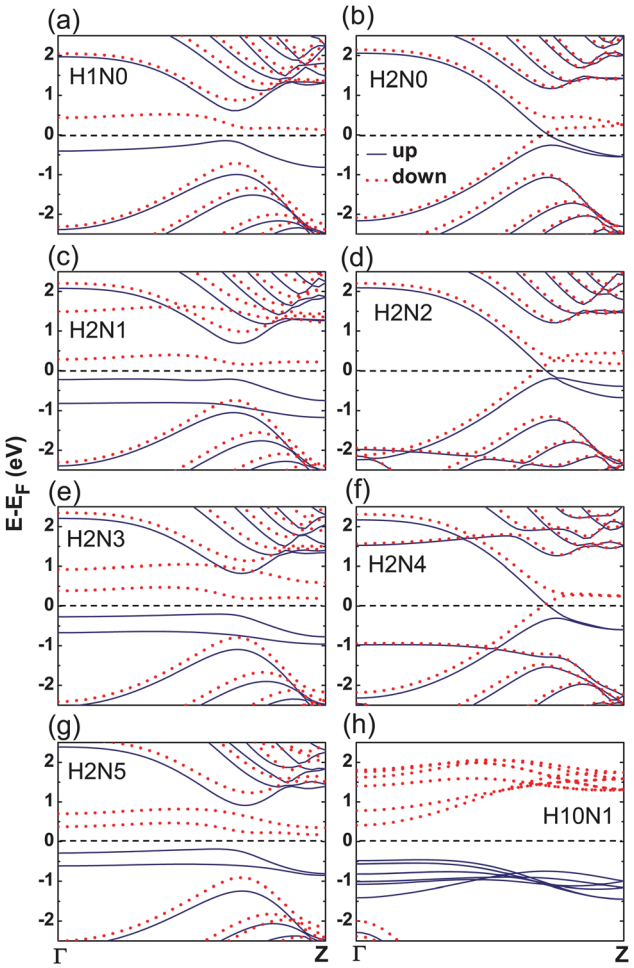

Fig. 4 The spin-dependent band structures for the systems of H1N0, H2N0, H2N1, H2N2, H2N3, H2N4, H2N5 and H10N1, respectively. Solid blue line: spin-up; dashed red line: spin-down. For each configuration, the valence orbitals of all the carbon and hydrogen atoms in the unit cell of the tube are used to construct the band structure. And the unit cells of those configurations are plotted in ESI.†

transmission features result from the band structure of the H1N0 tube, as shown in Fig. 4(a). It is the valence orbitals of all the carbon and hydrogen atoms in the unit cell of the tube (shown in ESI†) that are used to construct the band structure. From the figure, one finds that there are two bands around E_F (one for spin-up and one for spin-down), and they reside discretely on both sides of E_F. Obviously, it is these spin-up and spin-down bands that contribute to the corresponding spin-up and spin-down transmissions respectively, as shown in Fig. 3(d). The difference of Fermi distributions, $f_L(E,T_L) - f_R(E,T_R)$, mainly distributes in a small energy region around E_F, *i.e.*, $[-0.3, 0.3]$ eV, as shown in Fig. 3(c). In this energy region, the transmission of spin-up electrons distributes only above E_F. According to eqn (2), there will be a net spin-up current from the right to the left leads, *i.e.*, I_e. Similarly, a net spin-down current will flow in the opposite direction, *i.e.*, I_h. As a result, this leads to the emergence of the SSE.

In H1N0, the single H-line plays the role of a knife, cutting the tube into a curved graphene nanoribbon with two different types of edges, *i.e.*, zigzag and bearded ones. Previous studies show that more H-lines of linear hydrogenation in CNTs are realizable,[27,37] which may induce interesting electronic behaviors. So, it is necessary to investigate the tubes with more H-lines. In the present work, we mainly focus on the cases with two H-lines.

We constructed six two-H-line tubes, *i.e.*, H2Ny (y = 0–5), as shown in Fig. 1(b)–(g) respectively. From H2N0 to H2N5, the interval of the two H-lines becomes larger and larger. The corresponding spin-dependent currents are plotted in Fig. 2(b)–(g) respectively. One finds that all these systems exhibit the SSE. However, the variation trends of the spin current are quite different. They can be divided into two categories. One category is like the H1N0 tube, in which spin-up and spin-down currents increase simultaneously as T_L increases when $T_L > T_{th}$ (the flow directions of spin-up and spin-down currents are opposite). The currents exhibit a divergent form. As shown in the left panel of Fig. 2, H2N1, H2N3 and H2N5 (y in H2Ny is odd) belong to this category. The threshold temperature T_{th} of them is almost unchanged. We calculated the transmission spectra for all these cases (not shown), and found that they are all quite similar to that of H1N0. Thus, the interpretations of the currents for the configurations in this category are the same.

For another category (H2N0, H2N2 and H2N4, where y in H2Ny is even), when $T_L > T_{th}$, only one spin component of the currents increases and the other one remains almost zero as T_L increases. Taking H2N0 in Fig. 2(b) as an example, only the spin-up current increases when $T_L > 300$ K, and the spin-down current remains almost unchanged no matter how large the T_{LR} is. Only when $T_L > 500$ K the spin-down current (the absolute value) goes up but quite slowly. If we confine the working temperature to an upper limit of 500 K, such a system could be operated as a spin-Seebeck diode.

Apparently, an odd–even effect of the SSE emerges in such PHCNT systems. And it is interesting to figure out the underlying physical mechanism. In Fig. 4, we plot the band structures for the configurations mentioned above. Obviously, they can also be divided into two categories according to the parity of y in H2Ny. For H2Ny tubes with odd y, *i.e.*, H2N1, H2N3 and H2N5, the band structures show semi-conducting behaviors, and there are two or four (almost) flat bands residing discretely on both sides of E_F with opposite spins, like that of H1N0. However, for the tubes in another category (H2N0, H2N2 and H2N4), they are all metallic, and there are two bands possessing opposite spins across E_F. Comparing Fig. 2 and 4, one easily finds that there is a one-to-one correspondence between the currents and the band structures, where the metallic band structure corresponds to diode-like current and the semi-conducting band structure corresponds to divergent current.

For the latter category, we take H2N0 as an example and plot its transmission spectra in Fig. 3(e). For each spin component, there is one band across the Fermi level (Fig. 4(b)), so the transmission coefficient is 1.0 around E_F (the transmission channel is 100% opened). The difference of the transmission between spin-up and spin-down is actually located around E = 0.4 and −0.4 eV, as two bands meet in these energy regions for the spin-up or spin-down component (Fig. 4(b)). Two transmission peaks reside discretely on both sides of E_F with opposite spins, like the H1N0 case. But the peaks of H2N0 are farther away from the Fermi level than that of H1N0 (see Fig. 3(d) and (e)).

As mentioned above, it is the transmission difference between spin-up and spin-down that leads to the SSE, and the product of $[f_L(E,T_L) - f_R(E,T_R)]T_{\uparrow/\downarrow}$ plays an important role. However, $f_L(E,T_L) - f_R(E,T_R)$ mainly distributes in a small energy region around E_F, as shown in Fig. 3(c). Thus, the farther the transmission peaks are away from E_F, the smaller the product becomes. For H2N0, the spin-up transmission peak is closer to E_F than the spin-down one (Fig. 3(e)). It is easy to understand that the spin-up current is much larger than that of spin-down in Fig. 2(b), which is nearly zero. For H2N2 and H2N4 tubes, we also perform similar analyses and arrive at the same conclusion, *i.e.*, it is the asymmetry of the peaks relative to E_F for different spins that results in the diode effect.

The band structure is the key to the odd–even effect of the SSE. So it is necessary to figure out the origin of the band structures. Compared with the band structures of GNRs, one easily finds that those of H2N0, H2N2 and H2N4 are similar to that of GNRs in ferromagnetic (FM) state, especially for the bands around E_F. From a structural point of view, the tube could be seen as being divided into curved GNR parts by H-lines. It is necessary to explore whether the band structure of the tube is related to that of the GNR parts. We take H2N4 and H2N5 as examples respectively to study the two categories. Fig. 5 shows the band structures, as well as the isovalue surfaces of the spin charge density magnetization of them, for both tubes and GNR parts. The GNR structures have been saturated by hydrogen atoms at the "incision". The geometries after being cut have not been optimized, and this is only for the purpose of analysis (they may not be stable).

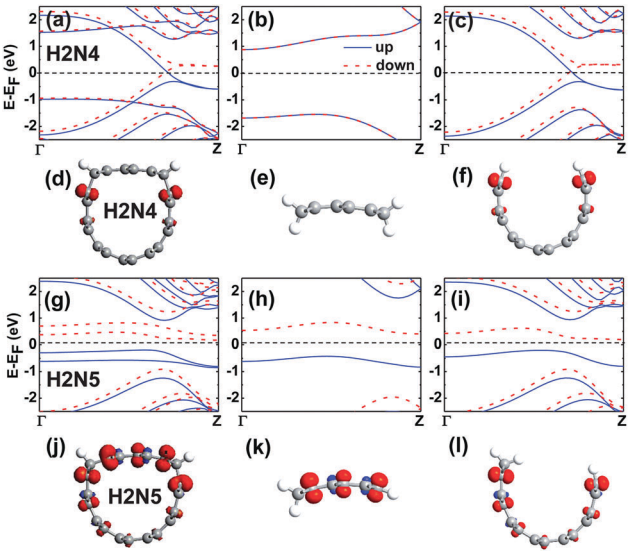

Fig. 5 (a) The spin-dependent band structures of the H2N4 system. (b and c) The spin-dependent band structures for the upper and lower parts of the H2N4 system, respectively, which could be seen as being cut off from the H2N4 tube. The structures in (b) and (c) have been saturated with hydrogen atoms for the carbon atoms at the "incision". The geometries after being cut have not been optimized, and this is only for the purpose of analysis (they may not be stable). (d–f) The corresponding configurations and their isovalue surfaces of the spin charge density magnetization for (a–c), respectively. (g–l) For the H2N5 system, similar to the H2N4 case in (a–f).

Comparing Fig. 5(a)–(c), it is clear that the band structure of the tube (Fig. 5(d)) is actually a combination of that of the two GNR parts (Fig. 5(e) and (f)). Note that the GNRs in Fig. 5(e) and (f) are obtained by cutting the tube in Fig. 5(d), and the GNRs in Fig. 5(k) and (l) are obtained by cutting the tube in Fig. 5(j). For H2N5, the same conclusion can be drawn (see Fig. 5(g)–(i)). As mentioned above, the "dividing" of a single H-line on a tube would create a zigzag and a bearded edge. According to the two edges of a ribbon, there will be three kinds of curved GNR parts, *i.e.*, zigzag–zigzag, zigzag–bearded and bearded–bearded. The GNR part in Fig. 5(f) is a zigzag–zigzag one. There are magnetic moments on both edges of it, like the zigzag GNR in FM state.[47] More importantly, it has quite a similar band structure (Fig. 5(c)) to isolated zigzag GNRs. For zigzag–bearded GNR parts in Fig. 5(h) and (i), although their width and degree of crimp are quite different, they exhibit almost the same electronic behaviors, *i.e.*, magnetism on edges and specific band structures (two bands reside discretely on both sides of E_F with opposite spins). Like H2N4, the band structure of the H2N5 tube is a combination of that of the two GNR parts (see Fig. 5(g)–(i)). That means the GNR parts have little influence on the electronic structure of each other in the tube, *i.e.*, the H-line almost cuts off the interaction between them.

As mentioned above, the diode effect is induced by the asymmetry of transmission peaks relative to E_F for different spins. And these peaks are contributed by the metallic bands, which actually come from zigzag–zigzag GNRs. So obtaining zigzag–zigzag GNRs by hydrogenation is the key to realize the spin-Seebeck diode. According to our denotation and

hydrogenating method, it is easy to understand that only when y in H2Ny is even (or zero), will there be zigzag GNR parts (divided by H-lines). This is the reason why only the configurations of H2N0, H2N2 and H2N4 exhibit the diode effect. And it could be considered as an odd–even effect of the SSE.

Furthermore, it is also possible to realize the SSE in a tube with more H-lines. As a demonstration, we construct a H10N1 tube which possesses ten H-lines. The geometry, spin-Seebeck current, transmission spectra and band structure of it are shown in Fig. 1(h), 2(h), 3(f) and 4(h) respectively. According to the positions of the H-lines, H10N1 belongs to the category which contains H2N1. And the results in these figures confirm our conclusion, *e.g.*, divergent spin-Seebeck current like that of H1N0. It should be noted that, compared with H2N1, more GNRs in H10N1 contribute to more flat bands around E_F and consequently result in more transmission channels and a larger transmission coefficient.

Therefore, the electronic features of an HxNy tube actually come from its GNR parts. The electronic behavior of a GNR mainly depends on the edges of it, robust to the width and degree of crimp. Thus it is easy to conclude that the nanotubes with other diameters are also suitable for such an application, and the odd–even SSE effect could also be expected in them (we have checked the (3,3) tubes and arrived at the same conclusion as with the (5,5) cases, see ESI† for details). Moreover, a variety of combinations of (maybe more than two) H-lines can be constructed, to realize more complicated applications. This provides us a feasible way to manipulate the SSE, and also to take advantage of the odd–even effect.

Conclusions

In summary, we studied the SSE in partially hydrogenated carbon nanotubes through first-principles calculations. It is found that linear hydrogenation in the CNT could make it acquire magnetism and exhibit an SSE. Moreover, an odd–even effect of the SSE is discovered, where the odd ones exhibit normal SSE behaviors and the even cases could be used as spin-Seebeck diodes. Further analysis shows that, the band structure of a tube is a combination of that of the GNR parts, which are divided by H-lines and the electronic behaviors of them depend on the edge type. It is the difference of band structures that results in the odd–even effect. More importantly, the mechanism could be extended to nanotubes with different diameters, showing great application potential. From a structural point of view, our PHCNT structure consists of only carbon and hydrogen atoms, which will be beneficial for device fabrication. The SSE and spin-Seebeck diode in our systems are realized and manipulated without the need for an electric field or gate voltage. We believe that our results would be helpful for developing nanotube-based spin caloritronics.

Conflicts of interest

There are no conflicts of interest to declare.

Acknowledgements

This work is supported by the National Natural Science Foundation of China (NSFC11504178, NSFC11374162, NSFC51651202 and NSFC11247033), the Natural Science Foundation of Jiangsu Province (BK20150825 and BK20170895), the Scientific Research Foundation of Nanjing University of Posts and Telecommunications (NY214010, NY217013 and NY214151), and the Fundamental Research Funds for the Central Universities (NS2014073).

References

1 X. Shi and L. Chen, *Nat. Mater.*, 2016, **15**, 691–692.
2 J. Plummer, *Nat. Mater.*, 2016, **15**, 127.
3 X. Crispin, *Nat. Energy*, 2016, **1**, 16037.
4 D. Awschalom and M. Flatt, *Nat. Phys.*, 2007, **3**, 153–159.
5 M. Brandbyge, J.-L. Mozos, P. Ordejn, J. Taylor and K. Stokbro, *Phys. Rev. B: Condens. Matter Mater. Phys.*, 2002, **65**, 165401.
6 A. Brataas, *Nature*, 2008, **452**, 419–420.
7 G. E. Bauer, E. Saitoh and B. J. van Wees, *Nat. Mater.*, 2012, **11**, 391–399.
8 K. Uchida, S. Takahashi, K. Harii, J. Ieda, W. Koshibae, K. Ando, S. Maekawa and E. Saitoh, *Nature*, 2008, **455**, 778–781.
9 T. Kimura, Y. Otani, T. Sato, S. Takahashi and S. Maekawa, *Phys. Rev. Lett.*, 2007, **98**, 156601.
10 S. O. Valenzuela and M. Tinkham, *Nature*, 2006, **442**, 176–179.
11 Y. Ni, K. Yao, H. Fu, G. Gao, S. Zhu and S. Wang, *Sci. Rep.*, 2013, **3**, 10547.
12 H.-H. Fu, D.-D. Wu, L. Gu, M. Wu and R. Wu, *Phys. Rev. B: Condens. Matter Mater. Phys.*, 2015, **92**, 045418.
13 Z.-Q. Zhang, Y.-R. Yang, H.-H. Fu and R. Wu, *Nanotechnology*, 2016, **27**, 505201.
14 S. Borlenghi, W. Wang, H. Fangohr, L. Bergqvist and A. Delin, *Phys. Rev. Lett.*, 2014, **112**, 047203.
15 T. L. Makarova, B. Sundqvist, R. Höhne, P. Esquinazi, Y. Kopelevich, P. Scharff, V. A. Davydov, L. S. Kashevarova and A. V. Rakhmanina, *Nature*, 2001, **413**, 716–718.
16 R.-H. Xie, G. W. Bryant and V. H. S. Jr., *Chem. Phys. Lett.*, 2003, **368**, 486–494.
17 M. Wierzbowska and A. Dominiak, *Carbon*, 2014, **80**, 255–267.
18 Y.-S. Liu, X.-F. Wang and F. Chi, *J. Phys. Chem. C*, 2013, **1**, 8046–8051.
19 M. Zeng, Y. Feng and G. Liang, *Nano Lett.*, 2011, **11**, 1369–1373.
20 Y.-S. Liu, X. Zhang, J.-F. Feng and X.-F. Wang, *Appl. Phys. Lett.*, 2014, **104**, 242412.
21 M. Zeng, W. Huang and G. Liang, *Nanoscale*, 2013, **5**, 200–208.
22 M. Schreier, N. Roschewsky, E. Dobler, S. Meyer, H. Huebl, R. Gross and S. T. Goennenwein, *Appl. Phys. Lett.*, 2013, **103**, 242404.
23 A. D. Avery, B. H. Zhou, J. Lee, E.-S. Lee, E. M. Miller, R. Ihly, D. Wesenberg, K. S. Mistry, S. L. Guillot and B. L. Zink, *et al.*, *Nat. Energy*, 2016, **1**, 16033.

24 C. A. Hewitt, A. B. Kaiser, S. Roth, M. Craps, R. Czerw and D. L. Carroll, *Nano Lett.*, 2012, **12**, 1307–1310.

25 W. Zhou, Q. Fan, Q. Zhang, K. Li, L. Cai, X. Gu, F. Yang, N. Zhang, Z. Xiao and H. Chen, *et al.*, *Small*, 2016, **12**, 3407–3414.

26 L. Xie, X. Wang, J. Lu, Z. Ni, Z. Luo, H. Mao, R. Wang, Y. Wang, H. Huang, D. Qi, R. Liu, T. Yu, Z. Shen, T. Wu, H. Peng, B. Ozyilmaz, K. Loh, A. T. S. Wee, Ariando and W. Chen, *Appl. Phys. Lett.*, 2011, **98**, 193113.

27 Ž. Šljivančanin, *Phys. Rev. B: Condens. Matter Mater. Phys.*, 2011, **84**, 085421.

28 M. Wierzbicki, R. Swirkowicz and J. Barnaś, *Phys. Rev. B: Condens. Matter Mater. Phys.*, 2013, **88**, 235434.

29 F. Muñoz Rojas, J. Fernández-Rossier and J. J. Palacios, *Phys. Rev. Lett.*, 2009, **102**, 136810.

30 M. Brandbyge, J.-L. Mozos, P. Ordejón, J. Taylor and K. Stokbro, *Phys. Rev. B: Condens. Matter Mater. Phys.*, 2002, **65**, 165401.

31 J. Taylor, H. Guo and J. Wang, *Phys. Rev. B: Condens. Matter Mater. Phys.*, 2001, **63**, 245407.

32 H. J. Monkhorst and J. D. Pack, *Phys. Rev. B: Solid State*, 1976, **13**, 5188–5192.

33 J. P. Perdew, K. Burke and M. Ernzerhof, *Phys. Rev. Lett.*, 1996, **77**, 3865–3868.

34 X.-F. Yang, Y.-S. Liu, J.-F. Feng and X.-F. Wang, *AIP Adv.*, 2014, **4**, 087116.

35 Y. Liu, X. Zhang, X. Yang, X. Hong, J. Feng, M. Si and X. Wang, *Phys. Chem. Chem. Phys.*, 2015, **17**, 10462–10467.

36 Q. Wu, P. Zhao, Y. Su, D. Liu and G. Chen, *RSC Adv.*, 2015, **5**, 20699–20703.

37 K. W. Lee and C. E. Lee, *Adv. Mater.*, 2012, **24**, 2019–2023.

38 W. Y. Kim and K. S. Kim, *Nat. Nanotechnol.*, 2008, **3**, 408–412.

39 O. V. Yazyev and M. Katsnelson, *Phys. Rev. Lett.*, 2008, **100**, 047209.

40 J. Dorantes-Dávila and G. M. Pastor, *Phys. Rev. Lett.*, 1998, **81**, 208–211.

41 Y.-W. Son, M. L. Cohen and S. G. Louie, *Phys. Rev. Lett.*, 2006, **97**, 216803.

42 P. Esquinazi, A. Setzer, R. Höhne, C. Semmelhack, Y. Kopelevich, D. Spemann, T. Butz, B. Kohlstrunk and M. Lösche, *Phys. Rev. B: Condens. Matter Mater. Phys.*, 2002, **66**, 024429.

43 Y. Kopelevich, P. Esquinazi, J. Torres and S. Moehlecke, *J. Low Temp. Phys.*, 2000, **119**, 691–702.

44 Y. Wang, Y. Huang, Y. Song, X. Zhang, Y. Ma, J. Liang and Y. Chen, *Nano Lett.*, 2008, **9**, 220–224.

45 O. V. Yazyev and L. Helm, *Phys. Rev. B: Condens. Matter Mater. Phys.*, 2007, **75**, 125408.

46 J. Červenka, M. Katsnelson and C. Flipse, *Nat. Phys.*, 2009, **5**, 840–844.

47 Y.-D. Guo, X.-H. Yan and Y. Xiao, *J. Appl. Phys.*, 2013, **113**, 244302.